Journal of Solid State Chemistry **149,** 209–217 (2000)
doi:10.1006/jssc.1999.8469, available online at http://www.idealibrary.com on IDEAL®

Color and Constitution of Cr^{VI}-Doped Bi_2O_3 Phases: The Structure of $Bi_{14}CrO_{24}$

S. A. Warda, W. Pietzuch, W. Massa, U. Kesper, and D. Reinen[1]

Fachbereich Chemie and Zentrum für Materialwissenschaften, Philipps-Universität, Hans-Meerwein-Strasse, D-35043 Marburg, Germany

Received April 30, 1999; in revised form July 28, 1999; accepted August 10, 1999

The structure of the deeply red chromium-doped Bi_2O_3 phase $Bi_{14}CrO_{24}$ is described: space group $I4/m$ ($Z = 2$); $a = 8.684$ (1) Å, $c = 17.238$ (1) Å. The Bi^{III} polyhedra show distinct distortions due to steric lone-pair effects. There is definite spectroscopic evidence that chromium is present as $Cr^{VI}O_4^{2-}$ tetrahedra, which occupy rather large cages in the lattice. They are only weakly tied to the frame of Bi^{III} cations—leading to distinct disorder phenomena. The red shift of the absorption edge with respect to the edge energies of the undoped Bi_2O_3 phases and the corresponding color effect are discussed as originating from a charge transfer process between Bi^{III} and Cr^{VI} via interconnecting oxygen atoms.

I. INTRODUCTION

Chromium (VI) stabilizes various phases, when doped into Bi_2O_3—depending on the chromium concentration. At low doping levels two compounds with the cubic Sillenite structure are observed, with lattice constants $a = 10.24$ (1) and 10.16 Å (2), respectively. The Sillenite structure is equivalent to the structure of γ-Bi_2O_3, one of the four modifications of Bi^{III} oxide. We will report on single crystal X-ray investigations on Cr^{VI}, Mo^{VI}, and S^{VI} doped Sillenite phases elsewhere (3).

A tetragonal compound of the approximate composition $Bi_{16}CrO_{27}$ with a broader homogeneity range—$x \cong 0.13 \pm 0.02_5$ for mixed crystal $Bi_{2-x}Cr_xO_{3+\delta}$, in agreement with our own powder diffraction investigations—and the unit cell parameters $a = 8.67$ Å, $c = 17.21$ Å (alternative space groups $I4$, $I\bar{4}$, $I4/m$) is reported by Zhitomirskii *et al.* (2). The single crystal X-ray studies reported here confirmed the existence of such a phase, but with the composition $Bi_{14}CrO_{24}$. The latter compound is apparently the stable phase within the mixed crystal range, because the single crystal synthesis always yields this composition, independent of x. The unit cell is claimed to be formally related to that of the tetragonal β-modification of Bi_2O_3 ($a_0 = 7.74$, $c_0 = 5.63$ Å; space group $P\bar{4}2_1c$ (4)) by $a \cong \sqrt{5}/2\, a_0$, $c \cong 3\, c_0$ (2). The structure of $Bi_{14}CrO_{24}$ is described in this contribution.

A further compound with the approximate composition $Bi_{10}Cr_2O_{21}$ exists in the $Bi_{2-x}Cr_xO_{3+\delta}$ series, with a reported rather broad homogeneity range of $x \cong 0.38 \pm 0.12$ as deduced from powder X-ray investigations and possessing the lattice constants $a' = 5.528(5)$ Å, $b' = 5.752(8)$ Å, $c' = 5.483(3)$ Å (2, 5). We could confirm the powder data in this case as well, with a narrower homogeneity range, however. The single crystal study revealed a very large supercell with $a = 3a'$, $b = 5b'$, $c = 3c'$, which did not allow us to solve the structure as yet.

Finally, Masuno reports about an orthorhombic phase $BiCrO_3$ with the lattice constants $a = 10.52$, $b = 17.63$, $c = 9.995$ Å (5). Depending on the preparation conditions, further compounds in the $Bi_{2-x}Cr_xO_{3+\delta}$ system can be isolated.

The colors of the described solids are orange-to-red, with the exception of $BiCrO_3$, which is green and apparently contains chromium in the +III oxidation state, at least partly. It is striking that the incorporation of chromium into Bi_2O_3 in lower concentrations leads to a significant lower-energy shift of the absorption edge as compared to the pale-yellow to orange-yellow hues, which characterize the pure Bi_2O_3 modifications. It is a further intention of this contribution to rationalize the mentioned red-shift in terms of a possible charge-transfer mechanism between Bi and Cr via the interconnecting oxygen ligands. While the Cr^{VI}-containing compounds are potential red pigments, analogous color shifts are not observed, if S^{VI} is the doping cation—though Sillenite and tetragonal phases similar to those of Cr^{VI} are stabilized. We will report on their properties here as well. Similar, though slightly smaller, lower-energy shifts of the absorption edge occur in compounds of Bi_2O_3 with ZrO_2 (3).

II. EXPERIMENTAL SECTION

A. Synthesis and Characterization

Carefully ground (ball mill) and dried mixtures of α-Bi_2O_3 and Cr_2O_3 (or CrO_2) in a molar Bi/Cr ratio of 14

[1]To whom correspondence should be addressed.

0022-4596/00 $35.00

were sintered as powders or tablets in corundum or platinum crucibles at 750°C in air for 1 day and cooled to room temperature for 4 h. After grinding, the heating procedure was repeated, resulting in the pure tetragonal $Bi_{14}CrO_{24}$ phase, with the unit cell parameters $a = 8.672$, $c = 17.21$ Å and a brilliant orange-red color.

Using $K_2S_2O_7$ as the doping material (Bi/S ratio: 7) and applying the same preparation conditions as those in the Cr case, we obtained a phase $Bi_{14}SO_{24}$, after K_2SO_4 had been removed by treatment with hot water. The unit cell parameters of the pale-yellow solid are $a = 8.648$ Å, $c = 17.24$ Å.

Structural powder X-ray analyses and optical measurements indicate that Cr^{VI} and S^{VI} can be mutually replaced by each other, with yellow-to-orange colors intermediate between those of the pure solids.

β-Bi_2O_3 was prepared by the decomposition of $(BiO)_2CO_3$ on a Pt plate at 380°C and was obtained as an orange powder.

γ-Bi_2O_3 was accessible from a KCl/NaCl melt with α-Bi_2O_3 as yellow single crystals by slowly cooling from 750 to 500°C (4°/h) and from 500° to 295°C in 2 h.

$Bi_{1.75}Zr_{0.25}O_{3+\delta}$ was synthesized from the stoichiometric mixture of α-Bi_2O_3 and ZrO_2, following the procedure described for the Cr^{VI}- and S^{VI}-doped compounds. The orange solid crystallizes in the β-Bi_2O_3 structure (6) with the lattice constants $a = 7.72$ Å, $c = 5.63$ Å. The homogeneity range of this phase in the mixed crystal series $Bi_{2-x}Zr_xO_{3+\delta}$ is $0.2 \leq x \leq 0.5$, without significant changes of the unit cell parameters dependent on x.

Single crystals of the tetragonal Cr^{VI} phase can be grown using powder samples $Bi_{14}CrO_{24}$, following either one of the following procedures: (a) cooling from the melt at 860°C with a rate of 4.8°/h to 600°C in a corundum or Pt crucible; (b) melting a mixture of the powder sample with KCl (2:5 weight ratio) at 800°C in a Pt crucible and cooling to 700°C at 2.2°/h and further to 300°C at 100°/h.

B. Single Crystal Diffraction Analysis

A red crystal of $Bi_{14}CrO_{24}$ was investigated on an IPDS area detector system. The crystal data and experimental conditions are given in Table 1. For an appropriate consideration of the very high absorption effect a careful numerical correction was performed (SHELXTL (8)) based on indexed crystal faces. Owing to the small size of the crystal and the absence of well-developed crystal faces an optimization of the crystal geometry was performed, based on a large number of equivalent reflections (9). The structure could be solved and refined in space group $I4/m$ with a disorder of the $Cr^{VI}O_4^{2-}$ tetrahedra as described in Section III. Refinement in the subgroup $I4$ did not result in a significant improvement; there was no indication of a possible merohedral twinning. The structure refinement against all F^2 data converged well at $wR_2 = 0.0826$, $R = 0.0456$ (for the observed reflections $wR_2 = 0.0813$, $R = 0.0372$).

TABLE 1
Measuring Conditions and Parameters for the X-Ray Analysis of $Bi_{14}CrO_{24}$

	Crystal data
Formula	$Bi_{14}CrO_{24}$
Crystal size (mm^3)	$0.1 \times 0.1 \times 0.18$
Absorption μ (mm^{-1})	94.85
Space group	$I4/m$ (No. 87), $Z = 2$
Lattice parameters (Å)	
a	8.684(1)
c	17.238(1)
Temperature (K)	293
D_c (g/cm^{-3})	8.588
	Data collection
Diffractometer	IPDS(Stoe) (8)
Radiation	Mo$K\alpha$ graphite monochromator (0.71073)
Measuring mode	$\Phi = 0$–$200°$, $\Delta = 1°$, $D = 40$ mm, $t = 10$ min/exp
Completeness	0.994
Theta range (deg.)	3.3–32.8; $\pm h$, $\pm k$, $\pm l$
Reflections (total/unique)	9400/1246 [$R_{(int)} = 0.112$]
	Computing
Refinement (7)	SHELXL-97
Atomic scattering factors	For neutral atoms, $\Delta f'$ and $\Delta f''$ from (9)
Absorption correction (8)	numerical
Extinction correction (7)	$\varepsilon = 0.00026(3)$
Refinement method	Full matrix least squares, $\sum w(F_o^2 - F_c^2)^2$ minimized
Number of parameters	60
$R_2(F^2)$, $R(F)$ (all refl.)	0.0826, 0.0456
Goodness of fit (F^2)	0.914
Max. ratio shift/esd	<0.001
$\Delta\rho_{max/min}$ ($e/Å^3$)	6.4, -4.5

The positional parameters and anisotropic displacement factors are listed in Table 2. Further details of the crystal structure investigation may be obtained from FACHINFORMATIONSZENTRUM KARLSRUHE, D-76344 Eggenstein-Leopoldshafen, Germany, by inquiring about the depository No. CSD-410882.

C. Spectroscopic Measurements

UV-vis spectra between 4000 and 28000 cm^{-1} were recorded using the powder reflection technique (Zeiss PMQII and Hitachi U-3410).

X-ray absorption near-edge structure (XANES) spectroscopy at the 1s-threshold of chromium-doped Bi_2O_3 pigments (10) was performed in Bonn (Prof. J. Hormes).

III. RESULTS AND DISCUSSION

A. Electronic Structure

Figure 1 presents the optical spectra of α-, β-, and γ-Bi_2O_3 inducing a yellowish, a pale orange, and again a faint yellow

TABLE 2
(a) Atomic Positions, (Equivalent) Isotropic Displacement Factors U [10^{-20} m^2 = Å^2], and Site Occupation Factors for $Bi_{14}CrO_{24}$ and (b) Anisotropic Displacement Factors of Bi, Cr, and O(1)–O(4)

(a) Atom	Position	x	y	z	U	s.o.f
Bi(1)	4*e*	0	0	0.6577(1)	0.0201(2)	1
Bi(2)	8*h*	0.7866(1)	0.5624(1)	0	0.0162(1)	1
Bi(3)	16*i*	0.7981(1)	0.6056(1)	0.6691(1)	0.0148(1)	1
O(1)	8*g*	0	0.5	0.3775(7)	0.024(2)	1
O(2)	16*i*	0.1225(9)	0.1828(9)	0.4218(5)	0.020(1)	1
O(3)	16*i*	−0.2524(9)	0.0772(10)	0.2562(5)	0.022(1)	1
Cr	4*e*	0	0	0.0188(5)	0.030(2)	0.5
O(4)	4*e*	0	0	0.111(2)	0.028(6)	0.5
O(5)	8*h*	0.153(14)	0.104(14)	0	0.041(8)	0.15(4)
O(6)	16*i*	0.154(7)	−0.065(7)	0.028(4)	0.041(8)	0.19(2)
O(7)	8*h*	0.199(8)	0.017(9)	0	0.041(8)	0.23(4)

(b) Atom	U_{11}	U_{22}	U_{33}	U_{23}	U_{13}	U_{12}
Bi(1)	0.0225(2)	0.0225(2)	0.0154(3)	0	0	0
Bi(2)	0.0120(2)	0.0169(2)	0.0196(2)	0	0	0.0010(2)
Bi(3)	0.0139(2)	0.0139(2)	0.0165(2)	0.0009(1)	−0.0006(1)	0.0006(1)
O(1)	0.018(4)	0.038(6)	0.017(4)	0	0	0.014(4)
O(2)	0.019(3)	0.021(3)	0.018(3)	−0.003(3)	−0.004(3)	0.004(2)
O(3)	0.020(3)	0.021(3)	0.025(4)	−0.008(3)	0.001(3)	0.001(3)
Cr	0.031(2)	0.031(2)	0.027(5)	0	0	0
O(4)	0.028(9)	0.028(9)	0.03(2)	0	0	0

color, respectively. The location of the absorption edge is rather steep in the case of the β-modification and corresponds to a semiconductor gap between the filled 6*s* and the empty 6*p* band of roughly 2.5 eV. In Fig. 2 the powder reflectance spectra of various Cr^{VI}, S^{VI}, and Zr^{IV}-doped Bi_2O_3 phases are collected. A distinct lower-energy shift of the absorption edge by about 0.5 eV with respect to that of β-Bi_2O_3 is observed on Cr^{VI} doping—the spectra of the Sillenite and the tetragonal and the orthorhombic phase (see the Introduction) being virtually identical. As a consequence orange-red to red colors occur. A similar, but somewhat smaller, edge shift is observed in the case of the orange mixed crystals between β-Bi_2O_3 and ZrO_2. In contrast, S^{VI} doping leads to nearly colorless solids, whose absorption edge is located around 23×10^3 cm^{-1}—in the region of those characteristic of α- and γ-Bi_2O_3 (Figs. 1 and 2).

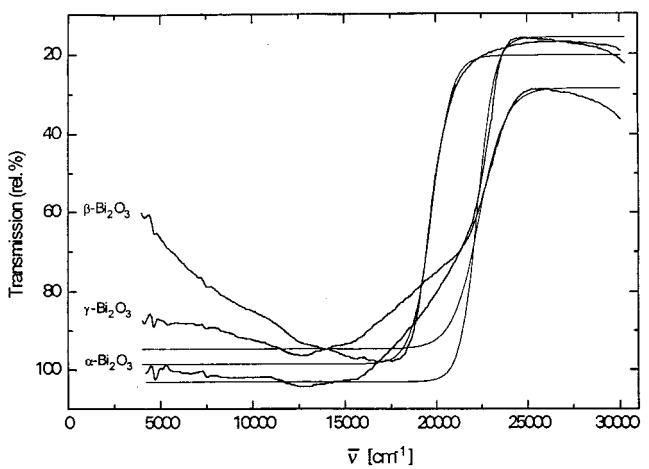

FIG. 1. Powder reflectance spectra of three Bi_2O_3 modifications (α, stable; β and γ, metastable at 298 K). The approximate turning points T of the absorption edges were determined by means of mean-square fitting curves, which are plotted with thin lines. T is 22.3, 19.8, and 22.4×10^3cm^{-1} for α-, β-, and γ-Bi_2O_3, with a margin of ± 250 cm^{-1}.

EPR spectroscopy of the Cr^{VI}-doped tetragonal solids yields a weak nearly isotropic signal, which further broadens on cooling. The g-value is slightly larger than 2.00, indicating unpaired electron density not bound to chromium, because otherwise g should be smaller than the spin-only value (11). Possibly low-lying impurity states are present, housing electrons, which are involved in a charge-transfer mechanism between Bi^{III} and Cr^{VI}. We will discuss in the next section whether the structural data are in favor of such a process.

The oxidation state of chromium in the orange-red to red tetragonal phases and cubic Sillenite compounds is + VI, and the coordination geometry is tetrahedral, as is unambigously deduced from iodometric titrations and by X-ray absorption spectroscopy at the Cr–K edge (10). It is in

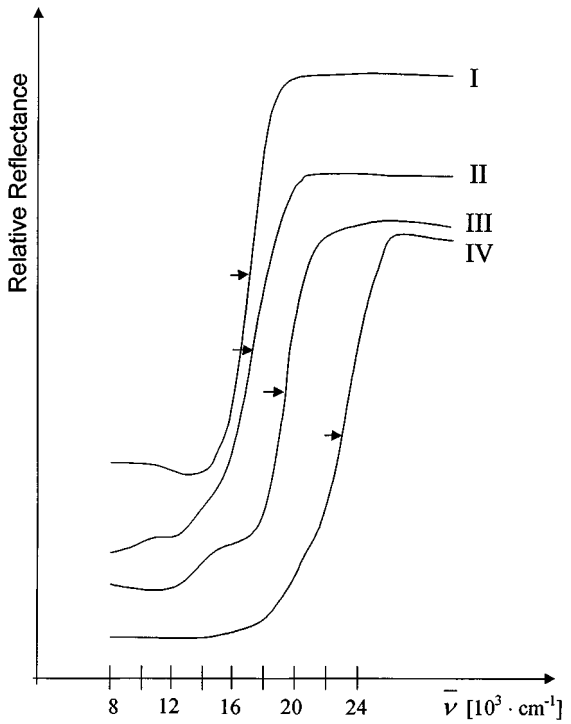

FIG. 2. Powder reflectance spectra of the tetragonal phases $Bi_{14}CrO_{24}$ (I) and $Bi_{14}SO_{24}$ (IV) and of a tetragonal mixed crystal $Bi_{1.75}Zr_{0.25}O_{3+\delta}$ (III). For comparison the spectrum of β-Bi_2O_3(II) is also shown. The turning points were determined as in Fig. 1 and occur at 16.8, 17.4, and 23.2×10^3 cm^{-1} for I, III, and IV, respectively, again with a margin of ± 250 cm^{-1}.

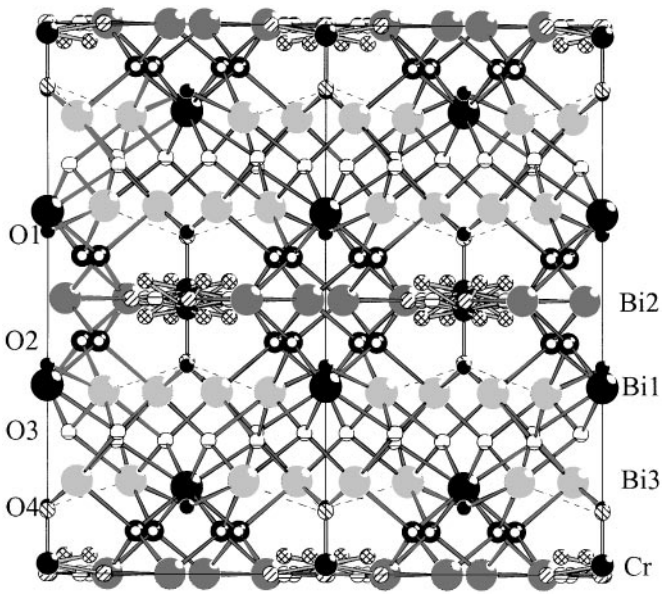

FIG. 3. The layer structure of $Bi_{14}CrO_{24}$, projected onto the *ac* plane. The unit cell is indicated; the element labels for the various atomic symbols are also given.

particular the location of the preedge peak—corresponding to an electronic $1s \rightarrow t_2$ ($3d$) excitation and appearing with high intensity only in the case of coordination geometries without inversion center—which sensitively reflects the oxidation state. The capability to distinguish between different oxidation numbers can be easily substantiated by comparison with the spectra of CrO_3 and $Ca_5(CrO_4)_3Cl$ containing $Cr^{VI}O_4^{2-}$ and $Cr^{V}O_4^{3-}$ tetrahedra, respectively (10). The presence of $Cr^{VI}O_4^{2-}$ polyhedra in the Cr-doped Bi_2O_3 solids is further confirmed by IR spectroscopy, namely, the presence of an intense band at 850 cm^{-1}. It can be assigned to the IR active τ_2 stretching vibration, red-shifted by $\cong 40$ cm^{-1} with respect to that of K_2CrO_4 (12)—presumably due to the bonding interactions of the oxygen atoms to Bi^{III} in the $Bi_{14}CrO_{24}$ lattice (see below). The location of this mode for $Cr^{V}O_4^{3-}$ is far off, at 765 cm^{-1} (12).

B. The Structure of $Bi_{14}CrO_{24}$

Figure 3 illustrates, in the projection along *b*, that $Bi_{14}CrO_{24}$ crystallizes in a layer structure, with Bi(2) plus Cr forming cationic sheets at $z \cong 0, 1/2$ and Bi(1) plus Bi(3) at $z \cong 1/6, 1/3, 2/3, 5/6$ (Table 2). While the oxygen atoms O(3) interconnect the latter layers, O(1), O(2), and O(4) bridge the two different types of cationic sheets. The interconnection pattern within the Bi(1), Bi(3) layers is illustrated by Fig. 4. The CrO_4^{2-} polyhedra occupy positions with $4/m$ site

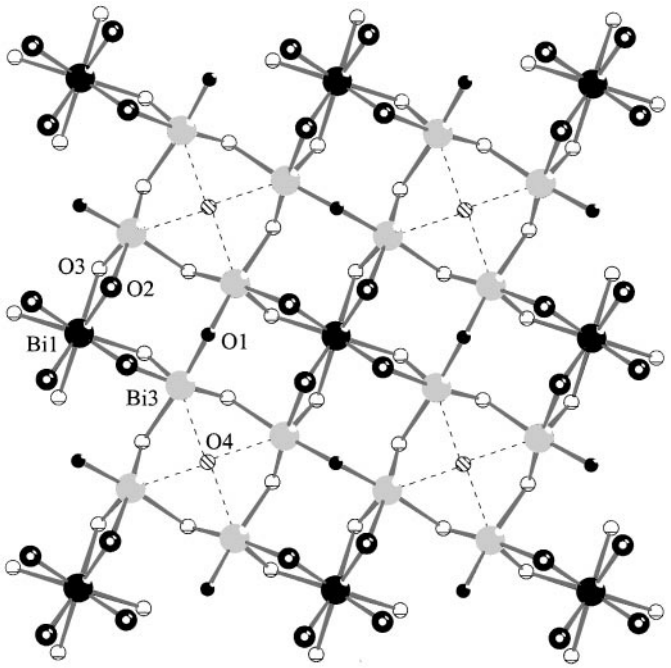

FIG. 4. View along the *c* direction of the $Bi_{14}CrO_{24}$ structure, with the Bi(1) and Bi(3) centers approximately in the paper plane.

symmetry within rather large cavities of the lattice, the coordinating O(4) to O(7) atoms being only weakly bonded to the neighbored Bi^{III} centers with Bi–O spacings between 2.8 and 3.2 Å. The Cr atoms are disordered over two neighbored positions on the C_4 axis above and below the mirror plane with a distance of 0.65 Å. According to the high symmetry of these positions and to the spectroscopic evidence for the presence of $Cr^{VI}O_4^{2-}$ tetrahedra, orientational disorder of the coordinated oxygen atoms has to be assumed as well. Only one of these, O(4)—located on the C_4 axis as Cr and also disordered over two positions—could be refined with anisotropic displacement factors of normal size. For the remaining oxygen atoms a very diffuse density distribution is found, concentrated in the mirror plane. Refinement with seemingly pseudo-octahedral geometry around Cr—using the highest maxima of the Fourier map only—led to extremely large anisotropic displacement factors (Fig. 5a). The best results have been obtained with the disorder model shown in Fig. 5b—based on three independent crystallographic sites O(5)–O(7), which correspond to a total of 16 oxygen positions (or 18, including O(4)) around Cr^{VI}. The O(5) and O(7) on the mirror plane and O(6) on a general position were refined with a common isotropic temperature factor, in order to avoid correlations with the occupation factors (Table 2). Because of the presence of the strongly scattering Bi atoms, it is not possible to refine the latter split positions with high accuracy. The proposed disorder model implies four possible orientations of $[Cr^{VI}$ O(4) O(5) O(6) O(7)$]^{2-}$ tetrahedra—alternatively for Cr^{VI} above or below the mirror plane. Two out of eight possible polyhedra are shown in Fig. 6. The spacings and bond angles within the tetrahedra are collected in Table 3. The former are 1.67(9) Å in the average, in good agreement with a reported Cr–O bond length of 1.65 Å in α-K_2CrO_4 (13). The averaged bond angle is $110 \pm 9°$. These data are sufficiently good to conclude that the proposed disorder model is reliable. One should finally mention, however, that the occupation of O(6) refines higher than that of O(7) and in particular O(5) (Table 2), this implying that not only [Cr O(4) O(5) O(6) O(7)]$^{2-}$ but also [Cr O(4), O(7), $O(6)_2$]$^{2-}$ tetrahedra might be involved in the disorder. Though the geometry of the latter tetrahedra appears to be rather distorted (O...O distances from 1.93 to 2.90 Å) as compared with the first type of tetrahedra (O...O distances from 2.57 to 3.06 Å), their presence can not be ruled out—having in mind that the refined positions of electron density maxima in such a complex disorder model may considerably deviate from the actual atomic positions of an individual polyhedron. Refinements with fixed occupation factors based on models with the first or second type of tetrahedra exclusively lead to a small increase of the wR_2 values.

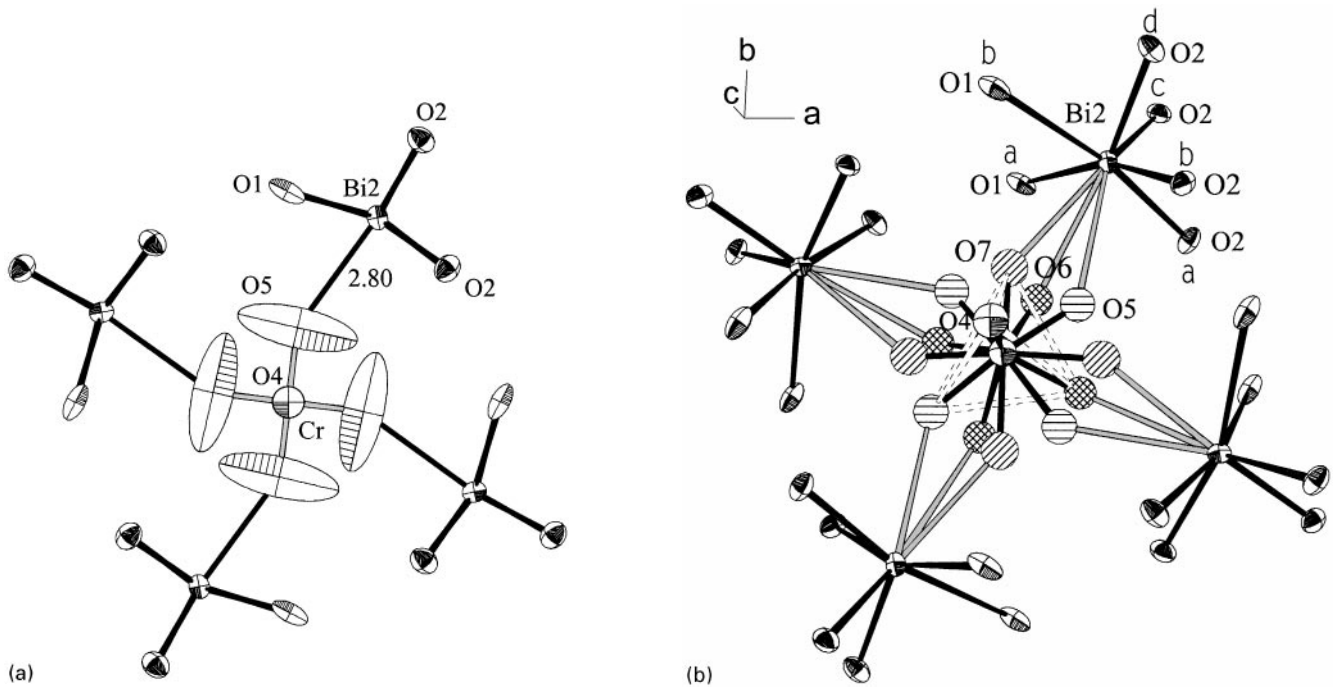

FIG. 5. View along the *c* direction of the $Bi_{14}CrO_{24}$ structure, with the Bi(2) and Cr cations located in the paper plane—situation before (a) and after (b) introducing the final disorder model. The Cr atom at $z = 0$ is strongly displaced along the C_4 axis in (a). In (b) the direction of projection is slightly canted with respect to *c*, in order to avoid superpositions of some of the Bi(2) oxygen ligator atoms. One possible Cr tetrahedron is indicated. The displacement ellipsoids are drawn here and in the subsequent figures at the 50% probability level.

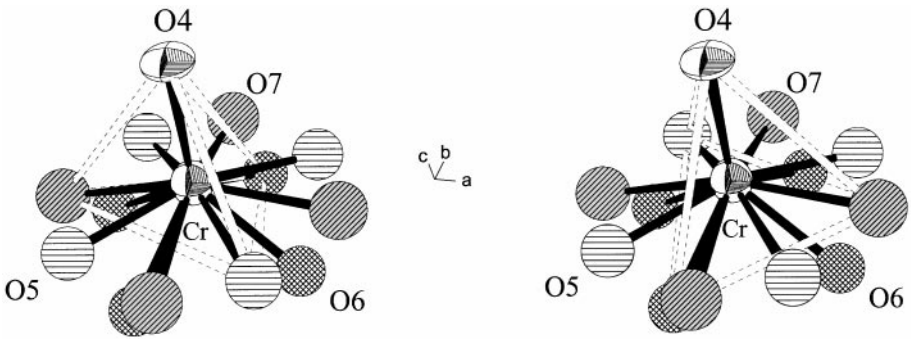

FIG. 6. The disordered CrO_4^{2-} tetrahedra for a chromium position above or below the mirror plane at $z = 0$ (see text); two possible orientations are shown.

There are three different Bi^{III} oxygen polyhedra in the lattice, whose geometries clearly indicate the presence of a lone pair with partial *p*-character at the metallic center. The ionic radius of Bi^{III} is such that coordination numbers of 6 and 8 versus oxygen ligator atoms are feasible. Indeed the parent geometry of the $Bi(1)O_8$ polyhedron is a cube, slightly rotated along one 4-fold axis toward an Archimedian antiprism. A distortion along the mentioned axis has occurred such that two groups of four Bi(1)–O bonds with short (2.35 Å) and long (2.73 Å) spacings, respectively, are generated (Fig. 7, Table 3). One may trace back this specific geometry to the lone pair of Bi^{III} extending along the 4-fold axis, repelling the O(3) ligands. Neglecting the oxygen atoms with distances > 2.8 Å for the present, Bi(2) is coordinated by four short-distance ($\cong 2.25$ Å) oxygen ligands in an arrangement very similar to that of $Bi(1)(O2)_4$ in Fig. 7, with an analogous lone-pair orientation (Fig. 8, Table 3). On the opposite side of the four short-bonded O(2) atoms one finds two additional O(1) and about one O(5) (or O(7) or O(6)) atoms at large distances from the Bi(2) center ($\cong 2.88(6)$ Å). The angles of the Bi(2)–O(5) (or (O6) or (O7)) bonds with respect to the presumable lone-pair direction are about $55^\circ \pm 15^\circ$, respectively.The parent coordination polyhedron of Bi(3) is apparently not a cube but an octahedron. If we consider only Bi–O distances below 2.8 Å, a square pyramid with a rather short axial spacing of 2.09 Å is apparent; here the equatorial plane is strongly distorted, implying two pairs of spacings with ≈ 2.2 and ≈ 2.6 Å, respectively (Fig. 9, Table 3). Neglecting this considerable bond-length anisotropy in the equatorial plane in a first rough consideration, the lone-pair should be oriented approximately opposite to the axial Bi(3)–O(3) bond. The additionally coordinated O(*i*) oxygen atoms from the CrO_4^{2-} polyhedron are bonded to Bi(3) with rather long distances of 2.93 Å(O(4) and $\cong 3.14$ Å (O(5), O(6), O(7)), forming angles of about 35° (O4) and $\approx 35 \pm 15^\circ$ (O(5), O(6), O(7)) in respect to the postulated lone-pair direction. These angles are even smaller if it is more realistically assumed that the lone-pair—according to the approximate C_s geometry of the Bi(3) polyhedron–is bent toward the long Bi(3)–O(2) and Bi(3)–O(3c) bonds, with an angle $< 180^\circ$ with respect to the short Bi(3)–O(3a) spacing (Fig. 9).

After all, the predominating distortion of the three coordination polyhedra occurs along a fourfold axis of a cube or octahedron, leading to geometries with an approximate C_{4v} symmetry (rather distorted in the case of Bi(3)), if Bi–O bond lengths > 2.8 Å are not taken into account. These situations can be qualitatively described by the steric lone-pair effect due to the Gillespie–Nyholm rules, but more thoroughly by a pseudo-Jahn–Teller effect. In the latter model the vibronic coupling between the ground state of Bi^{III} (A_{1g}–$6s^2$) and the first excited state T_{1u} ($6s^1p^1$) in O_h symmetry via vibrational τ_{1u} modes plays the crucial role (14). The $A_{1g} \otimes \tau_{1u} \otimes T_{1u}$ coupling and the corresponding ground state potential surface allows a rather precise analysis of the geometries and distortion pathways of the involved coordination polyhedra (15). This aspect will be followed elsewhere (16).

The cationic environment of the oxygen atoms O(1), O(2), O(3) corresponds to a more or less distorted tetrahedral Bi^{III} coordination, the $O(1)[Bi(2)_2Bi(3)_2]$, O(2)[Bi(1)Bi(2a) Bi(2b)Bi(3)], and O(3)[Bi(1)Bi(3a)Bi(3b)Bi(3c)] polyhedra possessing the bond distances and angles as given in Table 3. The O(4) is coordinated by four Bi^{III} and one Cr^{VI} cation, forming a compressed tetragonal pyramid. The O(5) binds one Cr^{VI} and three Bi^{III} cations, the latter with Bi–O spacings of ≈ 3 Å (Fig. 10). Though the angular deviations are very large, one may roughly describe the O(5) polyhedron as trigonally compressed—the cationic environment of O(6) and O(7) being similar (Fig. 10, Table 3).

The structure of $Bi_{14}CrO_{24}$ is singular and not related to the also tetragonal structure of β-Bi_2O_3 (4) in an obvious manner (see the Introduction). While the Bi^{III} ions in the latter compound possess the coordination number 6, the three different Bi^{III} centers in $Bi_{14}CrO_{24}$ are coordinated by 8, 6, and 5.5 oxygen atoms (Figs. 7–9), respectively, omitting

TABLE 3
Interatomic Distances (Å) and Angles (°) within the Three Bi^{III} Polyhedra and the $Cr^{VI}O_4^{2-}$-Tetrahedron of $Bi_{14}CrO_{24}$ (The Angles within the Polyhedra Formed by the Cationic Coordination of the O(*i*) atoms (*i* = 1 to 7) Are also Given.)

Bi(1)–O(2)	2.352(7)	(4 ×)	Bi(3)–O(3)a	2.086(8)	
Bi(1)–O(3)	2.730(8)	(4 ×)	Bi(3)–O(1)	2.136(4)	
			Bi(3)–O(3)b	2.221(8)	
Bi(2)–O(2)a	2.223(8)	(2 ×)	Bi(3)–O(2)	2.511(8)	
Bi(2)–O(2)b	2.282(8)	(2 ×)	Bi(3)–O(3)c	2.749(9)	
Bi(2)–O(6)	2.82(6)	(2 ×)	Bi(3)–O(4)	2.93(1)	
Bi(2)–O(1)	2.861(8)	(2 ×)	Bi(3)–O(5)	3.18(5)	
Bi(2)–O(7)	2.89(7)		Bi(3)–O(7)	3.14(3)	
Bi(2)–O(5)	2.94(12)		Bi(3)–O(6)a	3.10(6)	
			Bi(3)–O(6)b	3.19(6)	
Cr–O(4)	1.58(4)		Cr–Bi(3)	3.776(6)	(4 ×)
Cr–O(5)	1.64(11)	(4 ×)	Cr–Bi(2)	4.240(1)	(4 ×)
Cr–O(6)	1.67(6)	(4 ×)			
Cr–O(7)	1.76(7)	(4 ×)			
O(2)a–Bi(1)–O(2)b	70.1(2)	(4 ×)	Bi(3)–O(1)–Bi(3)	135.8(6)	
O(2)a–Bi(1)–O(2)d	108.7(4)	(2 ×)	Bi(2)–O(1)–Bi(2)	84.9(3)	
O(2)a–Bi(1)–O(3)a	70.3(3)	(4 ×)	Bi(3)–O(1)–Bi(2)	98.2(2)	(2 ×)
O(2)a–Bi(1)–O(3)b	120.9(3)	(4 ×)		113.6(2)	(2 ×)
O(2)a–Bi(1)–O(3)d	165.9(3)	(4 ×)			
O(2)a–Bi(1)–O(3)c	96.9(3)	(4 ×)	Bi(2)a–O(2)–Bi(3)	123.1(3)	
O(3)c–Bi(1)–O(3)b	72.8(2)	(4 ×)	Bi(2)a–O(2)–Bi(1)	109.0(3)	
O(3)a–Bi(1)–O(3)c	114.2(3)	(2 ×)	Bi(2)a–O(2)–Bi(2)b	106.1(3)	
			Bi(2)b–O(2)–Bi(1)	107.0(3)	
O(2)a–Bi(2)–O(2)b	74.7(4)		Bi(2)b–O(2)–Bi(3)	105.9(3)	
O(2)a–Bi(2)–O(2)c	73.7(4)	(2 ×)	Bi(3)–O(2)–Bi(1)	104.8(3)	
O(2)b–Bi(2)–O(2)c	115.9(4)	(2 ×)			
O(2)c–Bi(2)–O(2)d	72.4(4)		Bi(3)a–O(3)–Bi(3)b	133.1(4)	
O(2)c–Bi(2)–O(5)	140(1)	(2 ×)	Bi(3)a–O(3)–Bi(3)c	104.4(3)	
O(2)c–Bi(2)–O(7)	141.3(5)	(2 ×)	Bi(3)a–O(3)–Bi(1)	105.5(3)	
O(2)c–Bi(2)–O(6)a	134(1)	(2 ×)	Bi(3)b–O(3)–Bi(3)c	102.3(3)	
O(2)c–Bi(2)–O(6)b	154(1)	(2 ×)	Bi(3)b–O(3)–Bi(1)	109.6(3)	
			Bi(3)c–O(3)–Bi(1)	95.5(3)	
O(3)a–Bi(3)–O(1)	93.4(3)		Cr–O(4)–Bi(3)	110.2(7)	(4 ×)
O(3)a–Bi(3)–O(3)b	95.6(3)		Bi(3)–O(4)–Bi(3)	83.2(2)	(4 ×)
O(1)–Bi(3)–O(3)b	95.4(3)			140(1)	(2 ×)
O(3)a–Bi(3)–O(2)	79.0(3)				
O(1)–Bi(3)–O(2)	81.6(3)		Cr–O(5)–Bi(3)	98(2)	
O(3)b–Bi(3)–O(2)	173.7(3)			120(3)	
O(3)a–Bi(3)–O(3)c	75.6(3)		Cr–O(5)–Bi(2)	134(6)	
O(1)–Bi(3)–O(3)c	167.8(3)		Bi(3)–O(5)–Bi(3)	133(3)	
O(3)b–Bi(3)–O(3)c	80.7(4)		Bi(3)–O(5)–Bi(2)	86(2)	(2 ×)
O(2)–Bi(3)–O(3)c	101.1(3)				
O(3)a–Bi(3)–O(4)	149.0(5)		Cr–O(7)–Bi(3)	97(1)	
O(3)a–Bi(3)–O(6)a	166.7(12)			118(2)	
O(3)a–Bi(3)–O(7)	149.5(13)		Cr–O(7)–Bi(2)	130(4)	
O(3)a–Bi(3)–O(5)	141(2)		Bi(3)–O(7)–Bi(3)	137(2)	
O(3)a–Bi(3)–O(6)b	136.1(12)		Bi(3)–O(7)–Bi(2)	88(1)	(2 ×)
O(4)–Cr–O(5)	101.4(8)	(4 ×)			
O(4)–Cr–O(6)	119(2)	(4 ×)			
O(4)–Cr–O(7)	100.6(5)	(4 ×)			
O(5)–Cr–O(6)	112(4)	(4 ×)			
O(5)–Cr–O(7)	116(4)	(4 ×)			
O(6)–Cr–O(7)	108(3)	(4 ×)			

the Cr[(O(5)O(6)O(7)] grouping and taking the deficiency on the O(4) position into account. Furthermore the β-Bi_2O_3 structure possesses wide channels along [001], which may be occupied by cation and anion impurities (doping). The $Bi_{14}CrO_{24}$ structure, on the other hand, contains cages, which house the CrO_3 groups.

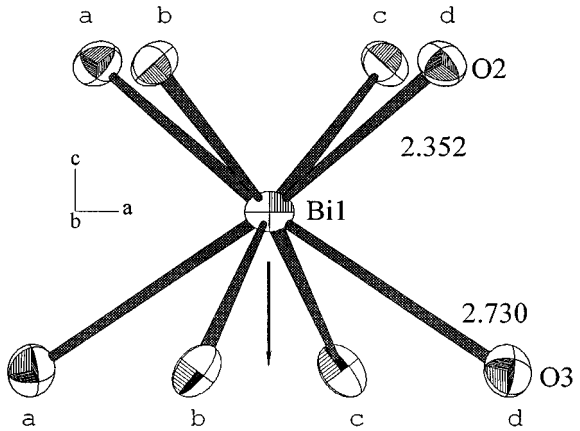

FIG. 7. The coordination geometry of the $Bi(1)O_8$ polyhedron (site symmetry $C_4 \| c$)—view along the *b*-axis. The presumable orientation of the lone-pair is indicated.

C. The Color Effect

We suppose that the considerable lower-energy shift of the absorption edge in the case of Cr^{VI}-doped Bi_2O_3 phases originates from an easy charge-transfer between Bi^{III} and Cr^{VI} via impurity states located in the semiconductor gap near the filled 6*s*(*p*)-valence band of $Bi_{14}CrO_{24}$. Functional density cluster calculations on structural fragments of this compound are in progress in order to check such a concept (16). The structural results indeed indicate a mechanism of this kind. The O(*i*) oxygen atoms ($i = 4$ to 7) strongly tied to Cr^{VI}, form additional weak bonds toward the $Bi(2)(O2)_4(O1)_2$ and $Bi(3)(O3)_3(O1)(O2)$ polyhedra (Figs. 8, 9) and are located in reach of the region, where the electron density of the lone-pair is presumably still high, as has been discussed

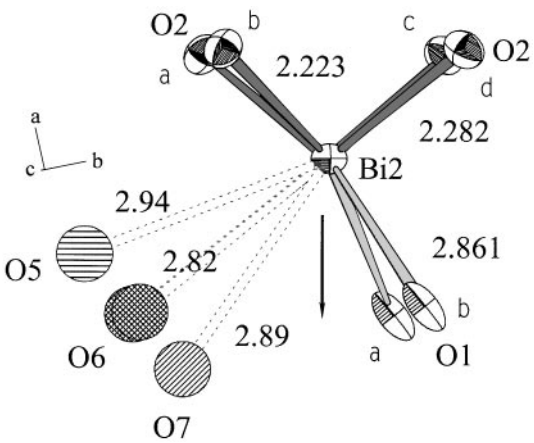

FIG. 8. The coordination geometry of Bi(2) with four short (O(2)) and further long-bonded (O(1); O(5) or O(6) or O(7)) oxygen atoms, projected along the *c*-axis. The site symmetry is $C_s(\perp c)$, with Bi(2), O(5), O(7) in this plane and O(6) very near this plane.

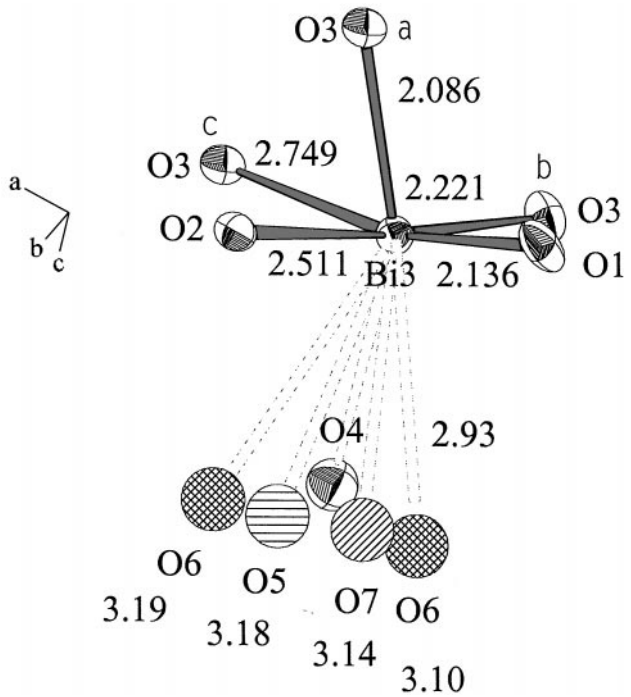

FIG. 9. The coordination geometry of Bi(3), approximating a distorted axially compressed tetragonal pyramid, with additional long-bonded (≈ 3 Å) oxygen atoms.

in the previous section. The O(4) is exclusively involved in the charge transfer between $Bi^{III}(3)$ and Cr^{VI}, while the O(*i*) with $i = 5$, 6, 7 seem to mediate such a process mainly between $Bi^{III}(2)$ and Cr^{VI}, counting only Bi(2)–O(4 to 7) spacings smaller than 3 Å ($\cong$2.88(6) Å; Figs. 8, 9). The Cr–O(4)–Bi(3) and Cr–O(5 or 6 or 7)–Bi(2) bond angles are 110(1)° and 135(6)°, respectively, and the Cr–Bi(3) and Cr–Bi(2) spacings are 3.78 and 4.24 Å (Table 3). Figure 3 illustrates that the process is 3-dimensional, with O(5), O(6), O(7) being active in the *a*–*b* planes and O(4) in the crystallographic *c*-direction. It is further noteworthy that the $Bi(1)O_8$ polyhedron, which exhibits the smallest pseudo-Jahn–Teller distortion and hence the most strongly screened lone-pair of the three Bi^{III} polyhedra, is not involved in the postulated transfer mechanism at all.

The missing color effect in the case of S^{VI}-doped Bi_2O_3 solids seems to have two reasons. On the one hand, the redox potential of Cr^{VI} is considerably higher than that of S^{VI}; on the other hand, a reduction of S^{VI} to S^{IV} would imply the presence of a lone-pair at the sulfur position and hence would destroy the tetrahedron geometry according to $S^{VI}O_4^{2-} \rightarrow |S^{IV}O_3^{2-}$. Chromium (VI) may accept one or two electrons from Bi^{III} without sterical implications; $Cr^{V}O_4^{3-}$ and $Cr^{IV}O_4^{4-}$ tetrahedra are well documented in the literature (11). The cavities, which house the CrO_4^{2-} tetrahedra, are large and flexible enough to accomodate to the expected bond length changes accompanying the

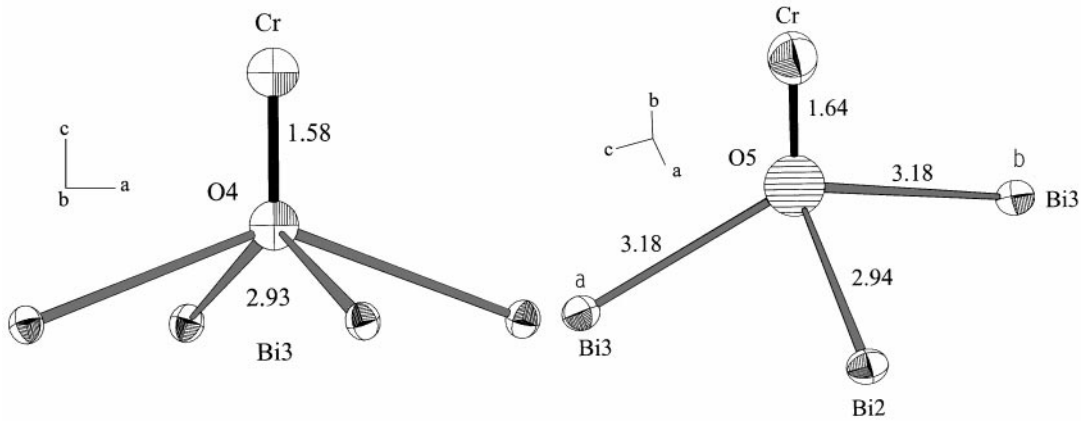

FIG. 10. The cationic coordination of the oxygen atoms O(4), with the Cr–O(4) bond on a C_4 axis, (left) and O(5), with Bi(2) and O(5) on a mirror plane, (right).

postulated electron density transfer from the lone-pair of Bi^{III} to Cr^{VI}—namely an expansion of the CrO_4^{2-} polyhedron and a motion of O(4) to O(7) toward the Bi(2) and Bi(3) centers. One should keep in mind, however, that the charge transfer is an excited state process; furthermore it is nonlocal, but cooperative throughout the lattice. In this connection it would be interesting to learn whether the disorder of the $Cr^{VI}O_4^{2-}$ tetrahedra is of static or dynamic nature. Our so-far structural single crystal investigations down to 190 K gave no evidence for an ordering process.

REFERENCES

1. Yu. F. Kargin, A. A. Mar'in, and V. M. Skorikov, *Inorg. Mater*. **18,** 1375 (1982).
2. I. D. Zhitomirskii, S. V. Fedotov, N. E. Skorokhodov, A. A. Bush, A. A. Mar'in, and Yu. N. Venetsev, *Russ. J. Inorg. Chem.* **28,** 570 (1983).
3. S. A. Warda, W. Pietzuch, W. Massa, and D. Reinen, in preparation.
4. S. K. Blower and C. Greaves, *Acta Crystallogr*. **44C,** 587 (1988).
5. K. Masuno, *J. Chem. Soc. Jpn.* (*Pure Chem. Section*) **90,** 1122 (1969).
6. F. Hund, *Z. Anorg. Allg. Chem.* **333,** 248 (1964).
7. SHELXTL, Release 5.05, Siemens Analytical X-Ray Instruments Inc., Madison,WI, USA, 1996; G. M. Sheldrick, SHELXL-97, Program for the Refinement of Crystal Structures, University of Göttingen, Germany, 1997.
8. IPDS Software Package, Stoe, Darmstadt, Germany, 1997.
9. "International Tables for Crystallography" (A. J. C. Wilson, Ed.), Vol. C. Kluwer Academic, Dordrecht, 1992.
10. A. Pantelouris, M. Pantelouris, J. Hormes, and D. Reinen, unpublished results.
11. D. Reinen, W. Rauw, U. Kesper, M. Atanasov, H. U. Güdel, M. Hazenkamp, and U. Oetliker, *J. Alloys Comp.* **246,** 193 (1997).
12. K. Nakamoto, "Infrared and Raman Spectra of Inorganic and Coordination Compounds," 5th ed., Part A. Wiley, New York, 1997.
13. K. Toriumi and Y. Saito, *Acta Crystallogr*. **B34,** 3149 (1978).
14. R. G. Pearson, "Symmetry Rules for Chemical Reactions—Orbital Topology and Elementary Processes." Wiley–Interscience, New York, 1976.
15. W. J. A. Maaskant and I. B. Bersuker, *J. Phys. Cond. Matter* **3,** 37 (1991).
16. M. Atanasov and D. Reinen, in preparation.